

UNVEILING THE MAIN HEATING SOURCES IN THE CEPHEUS A HW2 REGION

I. JIMÉNEZ-SERRA¹, J. MARTÍN-PINTADO², P. CASELLI¹, S. MARTÍN³, A. RODRÍGUEZ-FRANCO^{2,4}, C. CHANDLER⁵ AND J.M. WINTERS⁶

Draft version November 16, 2018

ABSTRACT

We present high angular resolution PdBI images (beam of $\sim 0.33''$) of the $J=27\rightarrow 26$ line from several vibrational levels ($v_7=1$ and $v_6=1$) of HC_3N toward Cepheus A HW2. These images reveal the two main heating sources in the cluster: one centered in the disk collimating the HW2 radio jet (the HW2 disk), and the other associated with a hot core $0.3''$ northeast HW2 (the HC). This is the first time that vibrationally excited emission of HC_3N is spatially resolved in a disk. The kinematics of this emission shows that the HW2 disk rotates following a Keplerian law. We derive the temperature profiles in the two objects from the excitation of HC_3N along the HW2 disk and the HC. These profiles reveal that both objects are centrally heated and show temperature gradients. The inner and hotter regions have temperatures of 350 ± 30 K and 270 ± 20 K for the HW2 disk and the HC, respectively. In the cooler and outer regions, the temperature drops to 250 ± 30 K in the HW2 disk, and to 220 ± 15 K in the HC. The estimated luminosity of the heating source of the HW2 disk is $\sim 2.2\times 10^4 L_\odot$, and $\sim 3000 L_\odot$ for the HC. The most massive protostar in the HW2 region is the powering source of the HW2 radio jet. We discuss the formation of multiple systems in this cluster. The proximity of the HC to HW2 suggest that these sources likely form a binary system of B stars, explaining the observed precession of the HW2 radio jet.

Subject headings: stars: formation — ISM: individual (Cepheus A) — ISM: molecules

1. INTRODUCTION

Cepheus A East, located at 700 pc (Reid et al. 2009) and with an IR luminosity of $\sim 2.5\times 10^4 L_\odot$ (Evans et al. 1981), is a very active star forming region with signposts of massive star formation (see e.g. Hughes & Wouterloot 1984). The brightest radio continuum source is the thermal radio jet HW2 (Rodríguez et al. 1994), which powers the northeast-southwest outflow seen in CO and HCO^+ (Narayanan & Walker 1996; Gómez et al. 1999).

Interferometric images of the molecular emission toward HW2 have revealed a very complex picture of the surroundings of the radio jet suggesting the presence of a cluster. Martín-Pintado et al. (2005), Patel et al. (2005), Brogan et al. (2007) and Comito et al. (2007) proposed that the number of sources in the HW2 system could be as many as five. Later, the higher-angular resolution observations of Jiménez-Serra et al. (2007) showed that the molecular gas around HW2 is resolved, at least, into a disk centered at the radio jet (the HW2 disk), and an independent hot core located at $\sim 0.4''$ east HW2 (the HC).

Brogan et al. (2007) reported vibrationally excited

emission of HC_3N (hereafter, HC_3N^*), previously detected by Martín-Pintado et al. (2005), arising from an unresolved condensation ($\leq 1''$; HW2-NE) located at the same position as the HC. The vibrational states of this molecule are excited mainly by IR radiation re-emitted by dust at $\lambda \leq 50 \mu\text{m}$. The determination of the size of the emitting region and of the excitation temperature of HC_3N provides a good estimate of the luminosity of the heating object (de Vicente et al. 2000). Brogan et al. (2007) derived a temperature of 312 K for the HW2-NE/HC source. Assuming a size of $\sim 0.6''$ for this object (Martín-Pintado et al. 2005), the expected IR luminosity is $\sim 2\times 10^4 L_\odot$. Since this luminosity is similar to that measured in HW2, and since the resolution of the Brogan et al. (2007) images is not high enough to discriminate between the HC and the HW2 source as the main heating source, the question remains whether HW2 or the HC is the most luminous source in the HW2 cluster.

We present high angular resolution PdBI images (beam of $\sim 0.33''$) of the $J=27\rightarrow 26$ rotational lines in the $v_7=1$ and $v_6=1$ vibrational levels of HC_3N , toward the Cepheus A HW2 region. The HW2 disk and the HC are centrally heated by two massive protostars. The central source of the HW2 disk is the most luminous object in the cluster.

2. OBSERVATIONS AND RESULTS

The $J=27\rightarrow 26$ $v_7=1_e$ and 1_f lines ($E_u/k=487$ K), and the $v_6=1_e$ and 1_f transitions ($E_u/k=883$ K)⁷ were observed simultaneously with the PdBI in the A configuration⁸. The correlator setup provided spectral resolutions

⁷ The v_7 and v_6 vibrational levels correspond to the bending modes of the C-C \equiv N and C \equiv C-C bonds.

⁸ Based on observations carried out with the IRAM Plateau de Bure Interferometer. IRAM is supported by INSU/CNRS (France), MPG (Germany) and IGN (Spain)

¹ School of Physics & Astronomy, E.C. Stoner Building, The University of Leeds, Leeds, LS2 9JT, UK; I.Jimenez-Serra@leeds.ac.uk, P.Caselli@leeds.ac.uk

² Centro de Astrobiología (CSIC/INTA), Ctra. de Torrejón a Ajalvir km 4, E-28850 Torrejón de Ardoz, Madrid, Spain; jmartin.pintado@iem.cfmac.csic.es, arturo@damir.iem.csic.es

³ Harvard-Smithsonian Center for Astrophysics, 60 Garden Street, Cambridge, MA 02138; smartin@cfa.harvard.edu

⁴ Escuela Universitaria de Óptica, Departamento de Matemática Aplicada (Biomatemática), Universidad Complutense de Madrid, Avda. Arcos de Jalón s/n, E-28037 Madrid, Spain

⁵ National Radio Astronomy Observatory, P.O. Box O Socorro NM 87801; cchandle@nrao.edu

⁶ Institut de Radio Astronomie Millimétrique, 300 Rue de la Piscine, F-38406 St. Martin d'Hères, France; winters@iram.fr

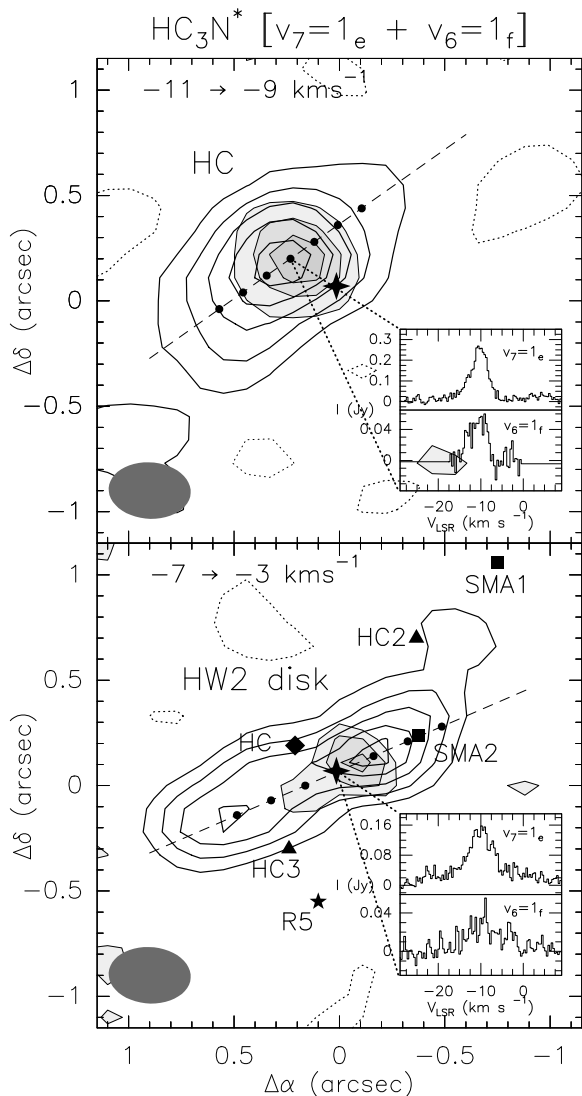


FIG. 1.— Integrated intensity images of the HC_3N^* $J=27\rightarrow 26$ $v_7=1_e$ (contours) and $v_6=1_f$ (grey scale and thin contours) line emission observed toward the HC (-11 to -9 km s^{-1} ; upper panel) and the HW2 disk (from -7 to -3 km s^{-1} ; lower panel). For the HC, the first contour and step level are 30 (3σ) and 50 mJy km s^{-1} for the $v_7=1_e$ map, and 10 (2σ) and 10 mJy km s^{-1} for the $v_6=1_f$ image. For the HW2 disk, the first contour and step level are 12 (2σ) and 12 mJy km s^{-1} for the $v_7=1_e$ emission, and 12 (2σ) and 6 mJy km s^{-1} for the $v_6=1_f$ line. Negative contours correspond to the 3σ level. The central coordinates are $[\alpha(J2000)=22^{\text{h}}56^{\text{m}}17.98^{\text{s}}$ and $\delta(J2000)=+62^{\circ}01'49.5'']$. Filled cross shows the expected location of HW2 (Curiel et al. 2006). The dashed lines and filled circles indicate the direction and positions at which the HC_3N^* excitation is calculated (Sec. 3). Beam size is shown at lower left corner. The spectra of the $v_7=1_e$ and $v_6=1_f$ lines toward the positions of the HC and the HW2 source are reported in the inner panels at lower right corner. We also show the location of the HC (filled diamond), SMA1 and SMA2 (filled squares; Brogan et al. 2007), HC2 and HC3 (filled triangles; Comito et al. 2007), and R5 (filled star; Torrelles et al. 2001) in the lower panel of this figure.

of ~ 80 and 160 kHz, i.e. ~ 0.1 - 0.2 km s^{-1} at 246 GHz. The synthesized beam size was $0.39'' \times 0.28''$ with a position angle (P.A.) of 85° . We used 3C454.3 (17 Jy) and 3C273 (11 Jy) as bandpass calibrators; MWC349 (1.3 Jy), as flux density calibrator; and 1928+738 (0.8 Jy)

and 0212+735 (0.7 Jy), as phase calibrators. Calibration, continuum subtraction, imaging and cleaning were done with the GILDAS package⁹.

The four HC_3N^* $v_7=1$ and $v_6=1$ transitions were detected toward HW2. In Figure 1, we show the integrated intensity maps of the $v_7=1_e$ (contours) and $v_6=1_f$ (grey scale and thin contours) emission from -11 to -9 km s^{-1} (the HC; upper panel), and from -7 to -3 km s^{-1} (the HW2 disk; lower panel). These lines are not blended, and therefore were mainly used in the analysis of our data. Figure 1 also shows the $v_7=1_e$ and $v_6=1_f$ spectra observed toward the HC and the HW2 source. In agreement with the SO_2 images of Jiménez-Serra et al. (2007), the HC_3N^* emission is resolved into two main molecular condensations: one centered at the HC, and the other associated with the protostellar disk around the HW2 jet, the HW2 disk. For completeness, we show in Figure 1 (lower panel) the location of sources SMA1, SMA2 (filled squares; Brogan et al. 2007), HC2, HC3 (filled triangles; Comito et al. 2007), and R5 (filled star; Torrelles et al. 2001) also reported in the region.

2.1. The Hot Core (HC)

The HC_3N^* emission from -11 to -9 km s^{-1} (upper panel, Figure 1) is relatively compact and mainly arises from the HC. The central radial velocity of this condensation is $v_{\text{LSR}} = -10$ km s^{-1} , and its peak emission is located at $\sim 0.3''$ north-east HW2. This position is similar to that reported by Martín-Pintado et al. (2005) for the HC, and consistent with the location of the HW2-NE source (Brogan et al. 2007). The deconvolved size of the $v_7=1_e$ line emission is $0.4'' \times 0.7''$ ($270 \text{ AU} \times 480 \text{ AU}$), and for the $v_6=1_f$ line, $0.25'' \times 0.4''$ ($170 \text{ AU} \times 270 \text{ AU}$). The HC is likely the powering source of the small-scale SiO outflow reported by Comito et al. (2007) toward HW2.

2.2. The HW2 disk

From -7 to -3 km s^{-1} , the HC_3N^* emission shows an elongated structure centered on HW2 that resembles the SO_2 disk reported by Jiménez-Serra et al. (2007). To our knowledge, this is the first time that high-excitation HC_3N^* lines are spatially resolved toward a protostellar disk. The HW2 disk is centered at $v_{\text{LSR}} = -5$ km s^{-1} , which gives a velocity difference between the HC and this object of ~ 5 km s^{-1} . This difference has also been observed in the circumstellar molecular gas around HW2 at larger scales (Codella et al. 2006).

While the HC_3N^* $v_7=1_e$ emission arises from all along the disk (deconvolved size of $1.4'' \times 0.18''$, $950 \text{ AU} \times 120 \text{ AU}$), the $v_6=1_f$ line is restricted to the inner and hotter regions closer to the HW2 source (size of $\leq 0.18'' \times 0.4''$, $\leq 120 \times 270 \text{ AU}$). The orientation of the $v_7=1_e$ and $v_6=1_f$ line emission (P.A. $\simeq 115^\circ$) is roughly perpendicular to the HW2 jet (P.A. $\simeq 46^\circ$; Rodríguez et al. 1994). This orientation, although not exactly the same, is similar to that seen in SO_2 , CH_3CN and NH_3 for the same velocity range (Torrelles et al. 2007). We note that Brogan et al. (2007) reported larger differences in the disk orientation for different molecular tracers. However, their molecular emission images were obtained for a larger velocity range from ~ -13 to

⁹ See <http://www.iram.fr/IRAMFR/GILDAS>.

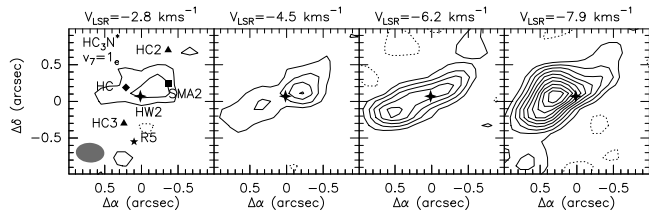


FIG. 2.— Images of the $\text{HC}_3\text{N}^* v_7=1_e$ emission observed toward HW2 for the velocity intervals from -2 to -3.7 km s^{-1} , -3.7 to -5.4 km s^{-1} , -5.4 to -7.1 km s^{-1} , and -7.0 to -8.9 km s^{-1} . The central radial velocities of these intervals are shown in the upper part of the panels. The first contour and step levels are $16 (2\sigma)$ and 16 mJy km s^{-1} . Symbols are as in Figure 1. Beam size is shown in the lower left corner.

0 km s^{-1} . In any case, the discrepancies in the disk orientation could be produced by either chemical or excitation effects.

The integrated intensity maps of the $v_7=1_e$ line for the velocity intervals of Jiménez-Serra et al. (2007), are shown in Figure 2. The kinematics of this emission are similar to those observed from SO_2 for the HW2 disk. The red-shifted HC_3N^* emission is brighter toward the northwest of HW2, and progressively moves to the southeast for blue-shifted velocities. The HC_3N^* emission at $V_{\text{LSR}} = -7.9 \text{ km s}^{-1}$ is clearly dominated by the HC. The velocity difference between the north-west and the south-east part of the HW2 disk is $\sim 5 \text{ km s}^{-1}$ over a projected distance of $\sim 1000 \text{ AU}$.

In Figure 3, we show the P-V diagram of the $v_7=1_e$ emission along the HW2 disk, after smoothing the data to a velocity resolution of 0.76 km s^{-1} . We also superpose the Keplerian rotation velocity curve for a star of $18 M_\odot$, a disk size of $\sim 1000 \text{ AU}$, and an inclination angle of the disk axis with respect to the line of sight of $\sim 62^\circ$ (Patel et al. 2005). Although the morphology of the HC_3N^* emission is very complex, the agreement of the data with Keplerian rotation (thick grey line) is particularly good for the red-shifted part of the HW2 disk. The blue-shifted part is contaminated by emission from the HC and shocked gas (Jiménez-Serra et al. 2007). Therefore, the HW2 disk seems to rotate following a Keplerian law. The central mass of $18 M_\odot$ is consistent with that estimated from the source size and the HC_3N^* excitation temperature for the HW2 disk (Section 4).

In contrast with the HW2 disk scenario, Brogan et al. (2007) reported chemical differences within the molecular structure around HW2 at $\sim 1''$ - $2''$ scales. These authors proposed that this feature could be instead due to the superposition of two independent objects in the plane of the sky. Although this possibility cannot be ruled out, there are several observational evidences that favour the disk scenario: i) HC_3N^* (this work), SO_2 and NH_3 (Jiménez-Serra et al. 2007; Torrelles et al. 2007), show a continuous structure whose kinematics are consistent with Keplerian rotation; ii) the observed HC_3N^* peaks do not seem to coincide with SMA1, HC2, HC3 or R5; for SMA2, this source falls $\sim 0.25''$ northwest the red-shifted HC_3N^* peak (we note that the uncertainty in absolute position is of $\leq 0.1''$); iii) the dust continuum emission delineates a similar structure to that seen in HC_3N^* , SO_2 or NH_3 (Torrelles et al. 2007); and iv) the spatial distribution of the H_2O and CH_3OH masers (Torrelles et al.

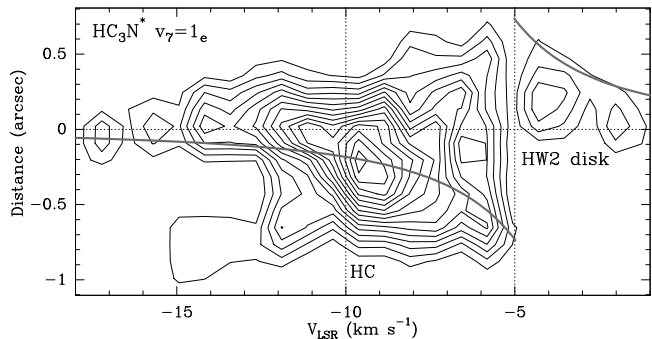


FIG. 3.— P-V diagram of the $\text{HC}_3\text{N}^* v_7=1_e$ emission along the HW2 disk. First contour and step level are $15 (3\sigma)$ and 10 mJy , respectively. Distances are calculated with respect to the HW2 source (horizontal dotted line; Curiel et al. 2006). Vertical dotted lines show the central radial velocities of the HW2 disk (-5 km s^{-1}) and of the HC (-5 km s^{-1}). The Keplerian rotation velocity for a central source with mass $18 M_\odot$, a disk size of $\sim 1000 \text{ AU}$, and an inclination angle of 62° , is also shown (thick grey line).

1996; Sugiyama et al. 2007), is consistent with the presence of a disk with radius ~ 600 - 700 AU . Therefore, we propose that the observed chemical differences within the HW2 disk could be produced by different external physical conditions, or by the presence of other hot core sources in the vicinity of HW2.

3. TEMPERATURE PROFILES AND HC_3N COLUMN DENSITIES

We can combine the $v_6=1$ and the $v_7=1$ lines of HC_3N to derive the excitation temperature of the hot gas along the HC and the HW2 disk (Figure 1) by means of Boltzmann diagrams. These diagrams assume LTE and optically thin emission. In case the v_7 lines were moderately optically thick, the derived excitation temperatures should be considered as upper limits.

Figure 4 shows the radial profile of the excitation temperatures of HC_3N toward the HC (filled triangles) and the HW2 disk (filled circles). The errors associated with these temperatures are $\leq 12\%$. For the HC, the temperature profile is centrally peaked with a maximum value of $270 \pm 20 \text{ K}$, and drops to excitation temperatures of $\leq 225 \text{ K}$ within the inner $0.15''$. This is consistent with the idea that the HC is internally heated by an IR source (see Figure 3 of de Vicente et al. 2002), and suggests that the hot gas is highly concentrated around the protostar. The temperature of 270 K is larger than that derived by Martín-Pintado et al. (2005, $\sim 160 \text{ K}$) from single-dish HC_3N data, but lower than that calculated by Brogan et al. (2007, $\sim 312 \text{ K}$). In the former, dilution effects could account for the temperature discrepancies. In the latter, the excitation temperature of $\sim 312 \text{ K}$ is only an upper limit, since the low lying HC_3N^* lines are likely optically thick (Brogan et al. 2007).

From the $v_7=1_e$ integrated line flux ($\sim 0.7 \text{ Jy km s}^{-1}$), and assuming a temperature of $\sim 220 \text{ K}$, the derived HC_3N column density in the HC is of $\sim 10^{16} \text{ cm}^{-2}$. The partition function of the $\text{HC}_3\text{N} v_7$ level has been calculated from the one in the ground vibrational state, but multiplied by ~ 0.3 . This corresponds to the factor $\exp[-(290 \text{ K}/220 \text{ K})]$, where 290 K is the energy of the fundamental rotational level in the v_7 state and 220 K is the derived excitation temperature. If we consider an

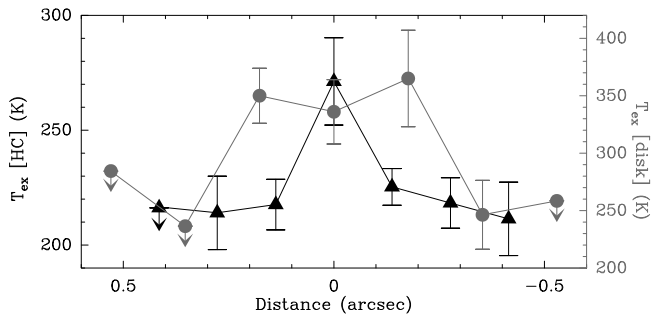


FIG. 4.— Radial distribution of the HC_3N excitation temperatures, with their errors, across the HC (filled triangles) and the HW2 disk (filled circles). The temperature scale for the HC is shown on the left, and for the HW2 disk, on the right. Arrows indicate the upper limits to the excitation temperatures of HC_3N .

HC_3N abundance of $\sim 10^{-8}$ (as for the Orion hot core; de Vicente et al. 2002), the estimated H_2 column density is $\sim 10^{24} \text{ cm}^{-2}$. Assuming a size of $\sim 0.5''$, this leads to a circumstellar mass of $\sim 0.6 M_\odot$ for the HC, which is consistent with that derived by Martín-Pintado et al. (2005) from SO_2 .

For the HW2 disk, the maximum excitation of HC_3N is found at $\sim 0.2''$ northwest and southeast of the radio jet (350 ± 40 and 365 ± 25 K, respectively), suggesting that the hot gas is distributed in an inner disk of radius $\sim 0.2''$ (140 AU; as estimated from Figure 4). Outside this disk, the temperature falls by more than 100 K. From the $v_7=1_e$ integrated line flux ($\sim 0.4 \text{ Jy km s}^{-1}$), and assuming a temperature of ~ 250 K, the derived column density of HC_3N is $\sim 3 \times 10^{16} \text{ cm}^{-2}$. By using Eq. 2 of Jiménez-Serra et al. (2007), and assuming an HC_3N abundance¹⁰ of $\sim 3 \times 10^{-10}$ – 10^{-9} , the estimated mass for the HW2 disk is ~ 0.4 – $1 M_\odot$. This mass is similar to that obtained by Patel et al. (2005), Jiménez-Serra et al. (2007) and Torrelles et al. (2007).

4. ON THE HEATING OF THE HC AND THE HW2 DISK

In the case of radiative excitation, the HC_3N gas temperatures are a good estimate of the dust temperatures because the continuum emission of the HC and the HW2 disk at 20 and $45 \mu\text{m}$ is likely optically thick. If we assume an H_2 column density of $\sim 10^{24} \text{ cm}^{-2}$, a gas-to-dust mass ratio of 100, and dust opacities of 3360 and $1810 \text{ cm}^2 \text{ g}^{-1}$ at 20 and $45 \mu\text{m}$ for both objects (Ossenkopf & Henning 1994), the derived optical depths are ≥ 60 . This explains the large obscuration seen toward HW2 at $24.5 \mu\text{m}$ by de Wit et al. (2009). Since gas and dust are thermally coupled, we can then estimate the IR luminosity of the central source by using the Stefan-Boltzmann law (de Vicente et al. 2000). From the $v_7=1$ emission size ($\sim 0.5''$), and considering spherical symmetry for the HC, we derive an IR luminosity of $\sim 3000 L_\odot$ for a dust temperature of 220 K. This luminosity, which is consistent with that obtained by Martín-Pintado et al. (2005), would correspond to a ZAMS B2-type star ($\sim 10 M_\odot$; Panagia 1973).

If we now consider an edge-on disk geometry with radius 475 AU and height 120 AU for the HW2 disk, we

estimate an IR luminosity of $2.2 \times 10^4 L_\odot$ for a dust temperature of 250 K. This is consistent with a ZAMS B0 star of $\sim 18 M_\odot$ for the HW2 source (Panagia 1973).

5. DISCUSSION

The high-angular resolution HC_3N^* images toward Cepheus A HW2 have shown that this multiple system contains two massive protostars. The powering source of the HW2 disk stands out among them with an IR luminosity of $2.2 \times 10^4 L_\odot$. The number of ionizing photons for a B0 star, as inferred from the heating ($\sim 10^{47} \text{ s}^{-1}$; Panagia 1973), is similar to that estimated by Hughes, Cohen & Garrington (1995) from the radio continuum emission of the HW2 radio jet ($\gg 5 \times 10^{46} \text{ s}^{-1}$). This indicates that the HW2 source is the most massive protostar in the region.

The mass of the HW2 disk, as derived from HC_3N , is relatively high (~ 0.4 – $1 M_\odot$) suggesting that this object is at an early stage of evolution. The dynamical age of the CO/HCO⁺ outflow ($\sim 5 \times 10^3$ yr; Narayanan & Walker 1996) is short compared to the lifetime of a photo-evaporating disk for a $\sim 18 M_\odot$ -star ($\leq 10^5$ yr; Gorti & Hollenbach 2009), suggesting that the HW2 disk probably constitutes the most massive disk associated with B stars detected so far (Fuente et al. 2003). The chemical differences observed within the HW2 disk (Brogan et al. 2007), could be due to different external physical conditions or to other hot core sources present within this multiple system.

The derived temperature profile for the HC indicates that this object is centrally heated by a protostar with an IR luminosity of $\sim 3000 L_\odot$. External heating of the HC would require luminosities of $\geq 10^5 L_\odot$ for the HW2 source as pointed out by Martín-Pintado et al. (2005). Shock heating could not account for the luminosity of the HC since the mechanical luminosity of the outflows in the region is only $\sim 40 L_\odot$ (Narayanan & Walker 1996). Therefore, the HC hosts a massive protostar. Since this object has not yet ionized its surroundings, the HC is at an earlier stage of evolution than the HW2 source.

Massive stars are usually found in binary systems (Mason et al. 1998). The proximity of the HC to HW2 (~ 200 AU) could be interpreted as a binary system. Coeval formation is likely the main mechanism for the formation of low-mass T-Tauri binaries (Ghez, White & Simon 1997). However, the orbits of these stars are preferentially aligned with the circumstellar disks of the primary stars (Jensen et al. 2004), which contrasts with the non-coplanarity of the HC/HW2 disk system. Alternatively, the HC could have formed after the fragmentation of the HW2 disk (Krumholz et al. 2009), but this would require disk-to-total-stellar mass ratios of ~ 0.1 – 0.2 , i.e. factors of 3 and 6 larger than that observed in HW2 (~ 0.03).

As shown by Cunningham et al. (2009), the capture of a massive companion (the HC) by the HW2 disk/protostar system in an eccentric orbit could explain the observed precession of the HW2 jet. If we assume an averaged orbital period of ~ 3700 yrs for the binary (Figure 7 in Cunningham et al. 2009), the expected mass enclosed within the system would be $\sim 25 M_\odot$ for a velocity difference of 5 km s^{-1} and an inclination angle of 62° . This mass is similar to the sum of the masses of the HC and the HW2 source as derived from HC_3N^* .

¹⁰ HC_3N is likely being photo-dissociated in the disk. The HC_3N abundance should be a factor of 10–30 lower than that found in the HC (e.g. Rodríguez-Franco et al. 1992).

Finally, we cannot rule out the idea that the formation of HW2 has triggered the formation of the HC and other objects in the region. Cepheus A HW2 therefore would resemble the case of SgrB2, where previous episodes of star formation triggered the formation of new clusters of massive hot cores (de Vicente et al. 2000).

In summary, we report the detection of HC_3N^* emission toward the HC and the HW2 disk in Cepheus A HW2. The HC_3N^* images show that these objects are centrally heated by massive protostars (of 18 and 10 M_{\odot} for the HW2 source and the HC, respectively). Since they appear to be very close (200 AU), we propose that

these objects form a binary system of massive stars.

We acknowledge the IRAM staff for the support provided during the observations. We thank two referees for their useful comments that helped to improve the paper, and W. J. de Wit and E. R. Parkin for fruitful discussions. JMP acknowledges the Spanish MEC for the support provided through projects number ESP2004-00665, ESP2007-65812-C02-01 and “Comunidad de Madrid” Government under PRICIT project S-0505/ESP-0277 (ASTROCAM).

REFERENCES

- Brogan, C. L., Chandler, C. J., Hunter, T. R., Shirley, Y. L., & Sarma, A. P. 2007, *ApJ*, 660, L133
- Codella, C., Bachiller, R., Benedettini, M., Caselli, P., Viti, S., & Wakelam, V. 2006, *MNRAS*, 361, 244
- Comito, C., Schilke, P., Endesfelder, U., Jiménez-Serra, I., & Martín-Pintado, J. 2007, *A&A*, 469, 207
- Cunningham, N. J., Moeckel, N., & Bally, J. 2009, *ApJ*, astro-ph:0902.2412
- Curiel, S., et al. 2006, *ApJ*, 638, 878
- de Wit, W. J., et al. 2009, *A&A*, 494, 157
- Evans, N. J., II, et al., 1981, *ApJ*, 244, 115
- Fuente, A., Rodríguez-Franco, A., Testi, L., Natta, A., Bachiller, R., & Neri, R. 2003, *ApJ*, 598, L39
- Ghez, A. M., White, R. J., & Simon, M. 1997, *ApJ*, 490, 353
- Gómez, J. F., Sargent, A. I., Torrelles, J. M., Ho, P. T. P., Rodríguez, L. F., Cantó, J., & Garay, G. 1999, *ApJ*, 514, 287
- Gorti, U., & Hollenbach, D. 2009, *ApJ*, 690, 1539
- Hughes, V. A., & Wouterloot, J. G. A. 1984, *ApJ*, 276, 204
- Hughes, V. A., Cohen, R. J., & Garrington S. 1995, *MNRAS*, 272, 469
- Jensen, E. L. N., Mathieu, R. D., Donar, A. X., & Dullingham, A. 2004, *ApJ*, 600, 789
- Jiménez-Serra, I., Martín-Pintado, J., Rodríguez-Franco, A., Chandler, C., Comito, C., & Schilke, P. 2007, *ApJ*, 661, L187
- Krumholz, M. R., Klein, R. I., McKee, C. F., Offner, S. S. R., & Cunningham, A. J. 2009, accepted, astro-ph:0901.3157
- Martín-Pintado, J., Jiménez-Serra, I., Rodríguez-Franco, A., Martín, S., & Thum, C. 2005, *ApJ*, 628, L61
- Mason, B. D., Gies, D. R., Hartkopf, W. I., Bagnuolo, W. G., Jr., ten Brummelaar, T., & McAlister, H. A. 1998, *AJ*, 115, 821
- Narayanan, G., & Walker, C. K. 1996, *ApJ*, 466, 844
- Ossenkopf, V., & Henning, Th. 1994, *A&A*, 291, 943
- Panagia, N. 1973, *AJ*, 78, 929
- Patel, N. A., et al. 2005, *Nature*, 437, 109
- Reid, M. J., et al. 2009, arXiv:0902.3913
- Rodríguez, L. F., Garay, G., Curiel, S., Ramírez, S., Torrelles, J. M., Gómez, Y., & Velázquez, A. 1994, *ApJ*, 430, L65
- Rodríguez-Franco, A., Martín-Pintado, J., Gómez-González, J., & Planesas, P. 1992, *A&A*, 264, 592
- Sugiyama, K., Fujisawa, K., Honma, M., Doi, A., Mochizuki, N., Murata, Y., & Isono, Y. 2007, in *Astrophysical Masers and their Environments*, IAU Symposium Proceedings (Ed. J.M. Chapman & W.A. Baan), 242
- Torrelles, J. M., Gómez, J. F., Rodríguez, L. F., Curiel, S., Ho, P. T. P., & Garay, G. 1996, *ApJ*, 457, L107
- Torrelles, J. M., et al. 2001, *ApJ*, 560, 853
- Torrelles, J. M., Patel, N. A., Curiel, S., Ho, P. T. P., Garay, G., & Rodríguez, L. F. 2007, *ApJ*, 666, L37
- de Vicente, P., Martín-Pintado, J., Neri, R., & Colom, P. 2000, *A&A*, 361, 1058
- de Vicente, P., Martín-Pintado, J., Neri, R., & Rodríguez-Franco, A. 2002, *ApJ*, 574, L163